Journal of Hydroscience and Hydraulic Engineering
Vol. 27, No.1 May, 2009, 105-119

EFFECT OF SLOPE MATERIAL PROPERTIES ON THE TIMING, SIZE AND PROCESSES OF LANDSLIDES

By

Daizo Tsutsumi

Disaster Prevention Research Institute, Kyoto University, Takayama, Gifu, Japan

and

Masaharu Fujita

Disaster Prevention Research Institute, Kyoto University, Gokasho Uji, Kyoto, Japan

SYNOPSIS

It is somewhat difficult to understand the process of landslides only by investigating the landslide scar after a landslide has occurred. Therefore, it is usually assumed that the shape of the landslide scar is formed only by a single slope failure. However, some recent landslides indicate that there is a different landslide process: multiple soil masses collapse one after another. In the present study, we refer to this kind of multiple soil mass failure as a "multi-phase landslide". It is not clearly understood what kind factors affect the multi-phase landslide occurrences, because they have not been studied. In this study, the effect of soil properties i.e., hydraulic properties and soil strength, on the process of the landslide occurrence including the multi-phase landslide are investigated by experimental and modeling approaches. The results of these investigations revealed that the soil layer with high internal friction angle and low cohesion tend to cause a small landslide, which might be followed by multi-phase landslides.

INTRODUCTION

Because it is unusual to witness slope failure itself, the process of the slope failure is usually determined by investigating the landslide scar after it has occurred. Therefore, morphology of the landslide scar is automatically regarded to be a slip surface of the landslide, and a single slope failure is usually presumed. A multi-phase slope failure, which is defined as several blocks of soil mass collapse one after another with certain time intervals, has not been considered except for special morphology of the landslide scars, such as discontinuous slope gradient. Furthermore, when the safety factor of a slope is once calculated to be unity, the shape of the calculated slip surface is presumed to be the final shape of the landslide in a conventional slope stability analysis. Therefore, the conventional slope stability analysis cannot reproduce or predict the multi-phase slope failure. However, several recent examples of slope failure indicate that the multi-phase slope failure usually occurs.

It can be stated that a multi-phase slope failure is more dangerous than a single-phase failure, because people have to sometimes approach the landslide area to rescue victims or to investigate a damaged house after the first

failure of the multi-phase slope failure, and might be attacked by second or third failures. To prevent the secondary damage by the multi-phase slope failure and to understand the process of the slope failure itself, it is important to investigate the mechanism of the multi-phase slope failure. In the present study, the mechanism of the multi-phase slope failure is examined by performing an experiment using an artificial slope and by carrying out a numerical simulation combining rain infiltration analysis and slope stability analysis, focusing on soil and hydraulic properties as affecting factors on multi-phase slope failure occurrence.

We can assume that various factors affect a multi-phase landslide occurrence, i.e., bedrock morphology, soil layer thickness, rainfall patterns, soil hydraulic properties and soil mechanical strength, and it is difficult to consider all these factors at a same time. Therefore, in the present study, we concentrated on the soil mechanical strength (i.e., internal friction angle ϕ and cohesion c) as the affecting factor to the landslide occurrence.

RECENT EXAMPLES OF MULTI-PHASE LANDSLIDE

Before discussing the experiment and numerical simulation regarding to the multi-phase slope failure, examples of actually occurred multi-phase slope failure in recent five years are introduced below.

Kasyu, Upstream area of the Nakagawa River, Tokushima Prefecture

Due to typhoon 0410 which hit Shikoku and Chugoku districts from July 31 to August 1, 2004, more than 1,000 mm total rainfall was recorded in the upstream area of the Nakagawa River, Tokushima Prefecture. This heavy rainstorm triggered a number of slope failures and caused serious sediment related disasters (1). One large slope failure occurrence in Kasyu area was witnessed from the opposite side of the river. According to a witness, several blocks of soil masses collapsed one after another from down-slope to up-slope gradually, and the total time from the beginning to the end of multi-phase slope failure was almost two days (see Fig. 1a).

Kotaki, Miyagawa RiverChatchment, Mie Prefecture

On September 29, 2004, a heavy rainfall due to typhoon 0421 caused a number of landslides in an upstream area of the Miyagawa River, Mie Prefecture. Seven people were killed or missing by the sediment related disaster (2). A slope failure occurred in the Kotaki area, Miyagawa Village (present Odai Town) and was witnessed from opposite side of the river. According to a witness, the lower 2/3 of the final length of landslide scar collapsed first, and the upper rest of the slope collapsed 20 minuets later (see Fig. 1b).

Minamikouchi, Taketa, Oita Prefecture

Typhoon 0514 hit Kyushu Island on September 2005, and more than 500 mm total rainfall from September 4 to 7 was recorded in Taketa, Oita Prefecture. Due to the heavy and long rainfall event, several large slope failures occurred in Taketa City. Two people were missing by a multi-phase slope failure occurred at Minamikouch area (3). According to residents, all residences were evacuated from the area and no one was left before the slope failure occurrence. Around 10:00 am September 6, a small slope failure occurred and a small amount of sediment had flown toward a house located at the foot of slope. Just after this first small slope failure, two residents of the house went back to check damage of their house. Around 11:30 am, while two residents stayed in their house, a second and larger slope failure occurred and the sediment hit the house and destroyed it completely (Fig. 1c). This is a typical example of a sediment disaster caused by a multi-phase landslide.

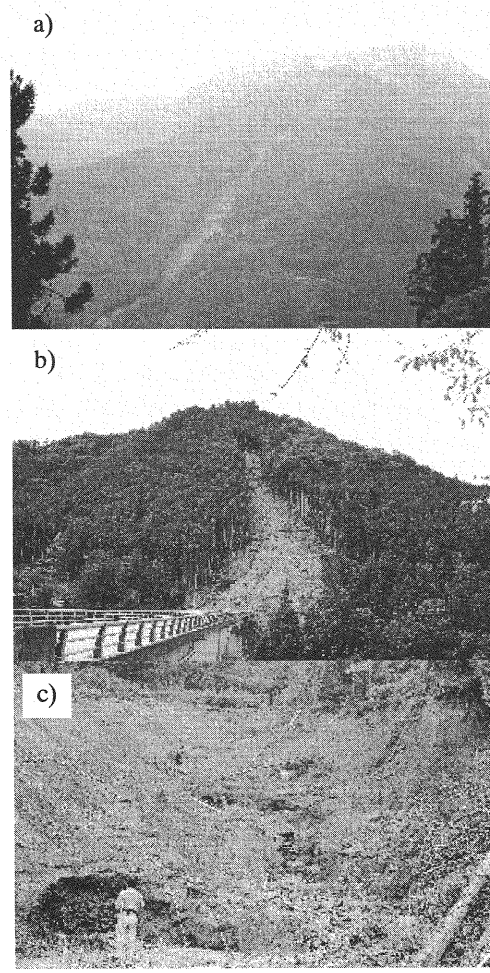

Fig. 1 Scars of multi-phase landslide occurred in a) Kasyu, Tokushima Pref., b) Kotaki, Mie Pref. and c) Minamikouchi, Oita Pref.

Comparing these examples, the size of each block of the multi-phase failure and the interval between each failure are different depending on the slopes. However, the process of the multi-phase slope failure, i.e. the lower part of the slope collapse first and the upper part of the slope collapse next due to the decrease of support at the lower part, seems to be same.

PHYSICAL EXPERIMENT OF LANDSLIDE USING ARTIFICAL SLOPE

Material and method of experiment

An experiment was conducted at Ujigawa Open Laboratory, Disaster Prevention Research Institute, Kyoto University. An experimental slope was prepared by filling a flume with soil. Artificial rainfall was applied to the soil surface of the slope. Fig. 2 illustrates a side view of the experimental slope and a sprinkler which produces the

artificial rainfall. As shown in Fig. 2, the length, depth, width and angle of the slope are 5.0 m, 0.3 m, 0.2 m and 30°, respectively. The right side wall of the flume is made of a transparent glass so that the soil displacement can be observed. Other boundaries of the flume: up-slope, down-slope, left side and bottom, are made of waterproof material. The bottom of the flume was pasted with silica sand No.3 to prevent losing friction between the soil layer and bottom of the flume. During the experiment, rainfall of 150 mm/hr was applied onto the surface of the sloped soil layer, and the pressure potential of bottom of the soil layer was continuously measured at six positions with tension-meters. Displacement and collapse of the slope were observed from the down-slope side and the right side of the slope and were recorded by a video camera.

Three types of experiments were conducted (Case 1, 2, and 3). For each case, a different type of soil was prepared and put into the flume. Actually measured mixing ratio of soil materials, parameters of the soil properties were listed in Table 1. Where, c' = cohesion, ϕ' = internal friction angle, K_s = saturated hydraulic conductivity, θ_s = saturated volumetric water content, θ_r = residual volumetric water content, σ and ψ_m = a dimensionless parameter related to the width of the pore-size distribution and the pressure potential corresponding to the median soil pore radius in Lognormal Model proposed by Kosugi (4), respectively. In Case 1, the soil has relatively high cohesion due to the pearl clay component mixed with the silica sand. In Case 2, the soil had no cohesion and exhibited quite high hydraulic conductivity due to the fact that there was no clay component mixing in the coarser silica sand. In Case 3, the soil also has no cohesion and high hydraulic conductivity which is lower than that in Case 2, due to mixing fine sand component in the coarse sand with ratio one to one. The flume was filled little by little with these soils, and hardened with a plate to control the slope hardness in the same way for every experimental case. The flume was set horizontally when the soil was filled. After filling the flume with soil, the soil layer was saturated and left horizontally for one hour. Subsequently, the flume was set 30° and left for 24 hours with the soil water being discharged from down slope end boundary opening to the atmosphere.

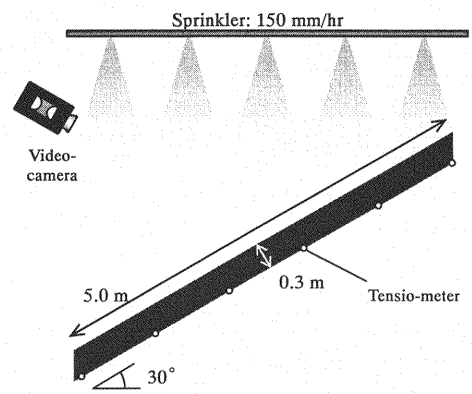

Fig. 2 Sectional drawing of artificial slope and sprinkler for landslide experiment

Table 1 Mixing rate of soils for experiments, and parameters of soil properties

	Case 1	Case 2	Case 3
SS3:SS6:PC*	80: 0: 20	100: 0: 0	50: 50: 0
c' [tf/m^2]	0.054	0	0
ϕ' [degree]	25	37	37
K_s [cm/sec]	0.050	0.567	0.079
θ_s [m^3/m^3]	0.481	0.405	0.365
θ_r [m^3/m^3]	0.138	0.032	0.046
σ [-]	1.090	0.699	0.580
ψ_m [cmH$_2$O]	-5.65	-4.25	-15.4

*SS3, 6 are the silica sand No.3 and 6, PC is the pearl clay

Table 2 Characteristics of experimental landslides

	Case 1	Case 2	Case 3
Occurrence	Yes	No	Yes
Time from beginning	15'05"	—	13'13"
Multi or single phase	Single	—	Multi

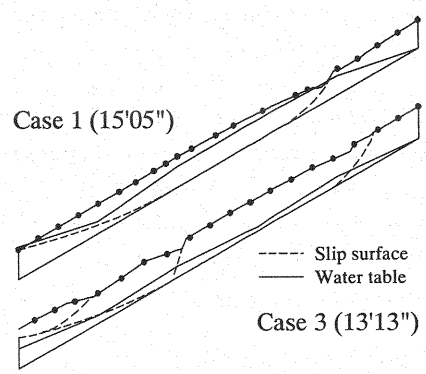

Fig. 3 Sectional drawing of experimental landslides
(At one second after the landslide occurrences)

Results of the experiment and discussions

The results of the experiment (slope failure occurrence, time from beginning to the occurrence, multi or single-phase slope failure) are listed in Table 2. In Case 1 and 3, slope failure occurred at 15'05" and 13'13" from the beginning of the experiment, respectively. However, in Case 2, no slope failure occurred for more than one hour rainfall application. The main reason for the slope stability in Case 2 might be that underground water table did not develop due to high hydraulic conductivity of the soil (see Table 1).

Configurations of slope surface and slip-surface were observed just after the slope failure occurrences in Case 1 and 3 which were shown in Fig. 3. When slope failure occurred in Case 1, a clack appeared around 4 m from the down-slope end, which was the upslope end of the slip surface, and resulting in the immediate collapse of the most part of the sloped layer. No slope failure following the first one was observed. When the slope failure occurred in

Case 3, a clack appeared around 1 m from the down-slope end, which was the upslope end of the slip surface of first slope failure, and the lower part of the sloped soil layer collapsed. Just after the first slope failure, the second and third slope failures occurred with the slip surface whose upslope end appeared at around 2 and 4 m above from down-slope end, respectively. The period of time from the first to the last slope failure was less than one second, and the final shape of landslide scar was quite similar to that of Case 1. However, the processes of the slope failure in Case 1 and 3 were different. In Case 3, because of the loss of support at foot of the slope due to the first collapse, the following second and third collapses might have occurred one after another. Therefore, the process of slope failure in Case 3 is the multi-phase slope failure in contrast to the single slope failure in Case 1. Because the only difference between Case 1 and 3 is the type of soil, the difference of the slope failure process may have been due to the properties of the soils.

Groundwater levels estimated from observed pore water pressure at the bottom of the sloped soil layer just before the slope failures in Case 1 and 3 are illustrated in Fig. 3. The groundwater level in Case 1 developed higher and wider than it in Case 3. Even the time of slope failure occurrences are almost the same in both Cases 1 and 3, the groundwater level in Case 1 is higher than that in Case 3. This may have been due to the higher hydraulic conductivity in Case 1 than in Case 3.

From the comparisons between Cases 1 and 3 shown above, mechanisms of the single and multi-phase slope failures are summarized below.

1) Single-phase slope failure

Because of the high cohesion of the soil, decrease in soil resistance against mass sliding due to the rise in groundwater level was comparatively small, and the groundwater can develop higher and wider until the resistance and sliding force becomes equivalent. Therefore, a large portion of the soil layer finally collapsed, due to the highly and widely developed groundwater table.

2) Multi-phase slope failure

Because there was almost no or very little cohesion of the soil, decrease in soil resistance in contrast to soil mass sliding due to rise of groundwater level was comparatively large, and the groundwater could not develop enough until the resistance and sliding force became equivalent. Therefore, the lower and smaller portion of the soil layer collapsed first, due to the limited development of groundwater table at lower part of the slope. However, because of the loss of support at foot of the slope due to the first collapse, the upper rest of the soil layer lost its stability and collapsed one after another in small portions. The timing of the slope failure occurrence is also dependent on the soil hydraulic properties.

CONSIDERATION BY MODELING APPROACH

The physical experiments of landslide shown in the previous section indicate that the process of landslide depends on their soil properties. However, because only three types of soil were used in the previous experiment, the general relationship between landslide process and soil properties has not been verified yet. In the present study, a numerical simulation was run to demonstrate the general relationship between the landslide process and the soil properties. At first, the simulation model was inspected by comparing the landslide processes obtained from the physical experiment and the numerical simulation. Next, two different hypothetic slopes were assumed and the landslide processes were simulated numerically with various combinations of soil properties. As a smaller hypothetic sloped soil layer, the one whose scale was the same as the previous physical experiment was employed (See Fig. 2). As a larger hypothetic soil layer, a slope with two horizontal parts jointed to the upslope and down-slope ends was assumed (See Fig. 4). Horizontal lengths of slope and horizontal parts were assumed 100 m and 15 m, respectively. The depth of the soil layer and the angle of the slope were assumed to be 2.0 m and 30°, respectively.

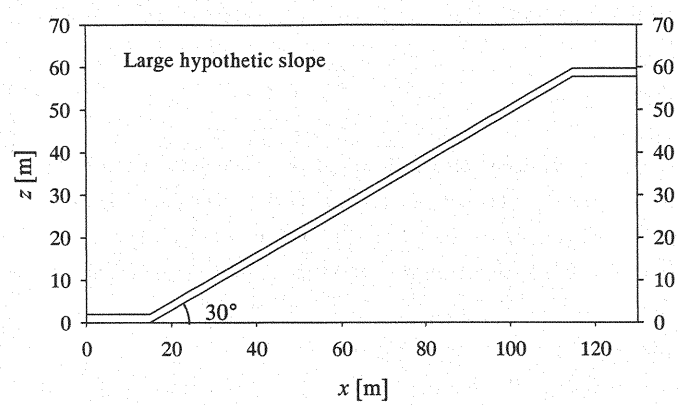

Fig. 4 Hypothetic large sloped soil layer for the model simulation

Table 3 Parameters of hydraulic properties of soils which were used for model simulation

Parameters	Common forest soil	Soil at Senokuchi, Oita Pref.
θ_s [m^3/m^3]	0.645	0.684
θ_r [m^3/m^3]	0.398	0.577
σ [-]	1.19	2.53
ψ_m [cmH_2O]	- 43.9	- 797.4
K_s [cm/sec]	0.005	0.0035

In the numerical simulation, a rainwater infiltration analysis and slope stability analysis were combined, and soil water infiltration within the soil layer and occurrence of slope failures were simulated. In the following subsection, detailed methods of the infiltration analysis and slope stability analysis are explained.

Method of rainwater infiltration analysis

The rainwater infiltration was calculated by solving the Richards equation shown below.

$$C(\psi)\frac{\partial \psi}{\partial t} = \nabla \cdot \{K(\psi)[\nabla(\psi + z)]\} \quad (1)$$

where, $C(\psi)$ = the soil water capacity and $K(\psi)$ = the hydraulic conductivity, which is represented by Lognormal model (4). The slopes were assumed to be two dimensional in x-z section, and divided into elements for the calculation of the finite element method (FEM). Measured hydraulic properties in the physical experiments (Table 1) were given for the hypothetic small slope. Two different hydraulic properties (one is assumed to be a common forest soil and another one is assumed to be soil which was sampled at a previous landslide scar; Senokuchi area landslide) were given for the hypothetic large slope (Table 3). For upslope, down-slope ends and bottom of the soil layer, no-flux boundary condition was imposed. Rainfall was applied to the soil surface. Rainfall intensities of 150 mm/hr and 40 mm/hr were imposed for small and large slope, respectively. Before the rainfall infiltration was calculated, the same procedures as the physical experiment was applied and calculated to control the initial moisture

condition in the soil layers for the small slope. For the large slope, similar procedure was calculated but the time for the soil water drainage was set to be 120 hr, while it was 24 hr for the small slope.

Method of slope stability analysis

The slope stability analysis was conducted simultaneously with the infiltration analysis. The simplified Janbu method was employed for the slope stability analysis, because it can be applied to any shape of slip surface. In the simplified Janbu method, the soil layer was divided into vertical slices, and the balance of stresses and slip condition within each slice are examined. The factor of safety F_s calculated by the simplified Janbu method is expressed as,

$$F_s = \frac{\sum\left[\{c_i' l_i \cos a_i + (W_i - u_i l_i \cos a_i)\tan\phi_i'\}/m_a\right]}{\sum W_i \tan a_i} \tag{2}$$

$$m_a = \cos^2 a_i\left(1 + \tan a_i \tan\phi_i'/F_s\right) \tag{3}$$

where, subscript i = number of vertical slice of soil layer, c_i' and ϕ_i' = cohesion and internal friction angle of the soil, W_i = weight of the slice, a_i and l_i = angle and length of slip surface within the slice, and u_i = the water pressure affected on the slip surface.

Following a previous study by Kubota and Nakamura (5), Dynamic Programming method (DP method) was utilized to seek out the slip surface which provides a minimum factor of safety. Spatial distribution of the pore water pressure, which was calculated by the rainwater infiltration analysis, was used in the slope stability analysis as input data. Measured internal friction angle ϕ' and cohesion c' of the soil were given for the model inspection by simulating the physical experiment (see Table 1). For the calculation with the hypothetic slopes, various combinations of ϕ' ($15° \leqq \phi' \leqq 40°$, with an interval of 1°) and c' ($0.00 \leqq c' \leqq 2.0$ tf/m^2, with an interval of 0.01 tf/m^2) were given. For every combination of properties, the occurrence of slope failure, the time of the slope failure occurrence and the size of the first slope failure were recorded, and the relationship between the soil properties and landslide processes was examined.

Results of model simulation and discussions

The landslides were simulated 25 and 22 minutes after the rainfall application started in Case 1 and 3, respectively. Sectional shape of calculated slip surfaces were illustrated in Fig. 5. According to the calculated results, almost all the soil layer collapsed at once in Case 1, and only a small portion of the soil layer at the down-slope end of the slope was collapsed in Case 3. Compared to the results of the physical experiment, the size of the slope failure calculated for Case 1 and time of landslide occurrences in Case 1 and 3 were a little overestimated, the overall tendencies of the landslide occurrence in both cases were well simulated. Therefore, reliability of the simulation method employed in the present study was confirmed.

Counter curved drawings of simulated time of slope failure occurrences and size of the slope failure (ratio of sectional area above slip surface to total sectional area of soil layer) for various combination of ϕ' and c' assuming the small slope were illustrated in Figs. 6 and 7, respectively. Landslide occurrence was calculated at initial condition in the triangle regions I shown in Fig. 6. This means that a slope (with the soil properties shown in the triangle region I) does not exist. On the other hand, no landslide occurrence was calculated in the triangle regions II shown in Fig. 6. From these results, we think there is little meaning in considering not only the timing of landslides in these regions

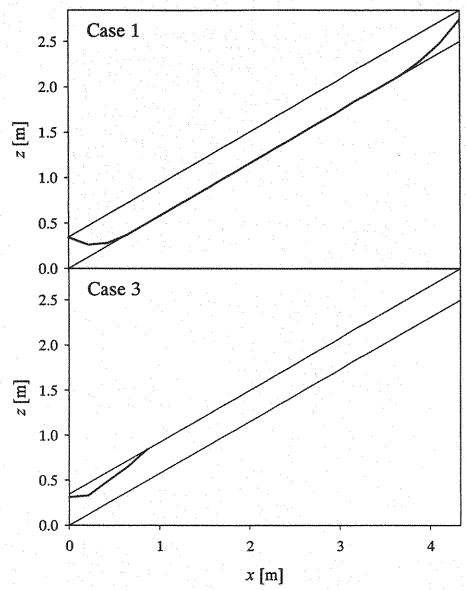

Fig. 5 Simulated slip surface for landslide experiments, Case 1 and 3

shown in Fig. 6, but also the size of landslides in these regions shown in Fig. 7. Therefore, the simulated results shown in these regions I and II were excluded from the discussions of Figs. 6 and 7. The hydraulic properties of the soil used in the physical experiment in Case 1 and 3 were given in the numerical simulation and each finding is illustrated in the upper figure (a) and lower figure (b), respectively. Fig. 6 indicates that the time of landslide occurrence became longer as the soil strength ϕ' and c' became larger in both Cases 1 and 3. It is a natural tendency that a soil layer becomes more tolerant to sliding force when the soil strength is greater. Fig. 7 shows that the size of slope failure became smaller as ϕ' became larger and c' became smaller in both Cases 1 and 3. Therefore, even if a landslide occurs at a same time, the size of the landslide will be different depending on the combination of ϕ' and c'.

Simulated time of slope failure occurrences and size of the slope failure assuming large slope were illustrated in Figs. 8 and 9, respectively. The simulated results shown in these regions I and II were not included in the discussions of Figs. 8 and 9, for the same reason as Figs. 6 and 7. Similar to the small slope (Fig. 6), Fig. 8 indicates that the time of landslide occurrence became longer as the soil strength ϕ' and c' became larger in both Cases 1 and 3. By comparing the results for the common forest soil (Fig. 8a) and Senokuchi soil (Fig. 8b), we can observe that the landslide occurred much later in the common forest soil layer. This tendency is due to the high hydraulic conductivity of the forest soil. Similar to the small slope (Fig. 7), Fig. 9 indicates that the size of the slope failure became smaller as ϕ' became larger and c' become smaller for both assumed soil layer. By comparing the small and large scaled slope, we found that the relative size of the slope failure in the large slope was smaller than that in the small slope. According to the calculated shape of landslide, every slip surface has its shape whose lower end is at the down-slope end of the slope.

The results of the numerical simulation discussed above suggest that a relatively small portion at down-slope end of slope with small soil cohesion c', which means the slope was kept stable mainly by soil internal friction angle ϕ', tends to collapse and is followed by following multi-phase failures. On the other hand, a relatively large portion of the slope with small soil internal friction angle ϕ', which means the slope was kept stable mainly by soil cohesion c', tends to collapse at once and is not followed by a slope failure. These tendencies may have been due to the same

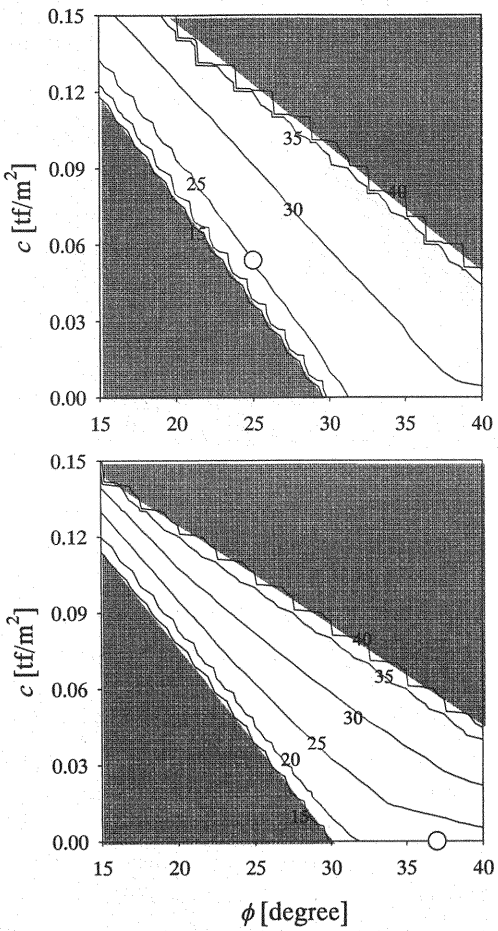

Fig. 6 Calculated relationships between time from rainfall beginning to collapse occurrence and soil strength assuming experimental slopes (a: Case 1, b: Case 3, white circles ○ indicate experimental results)

reason as the physical experiment discussed above. The hydraulic properties of the soil also affect the processes of a single or multi-phase slope failure.

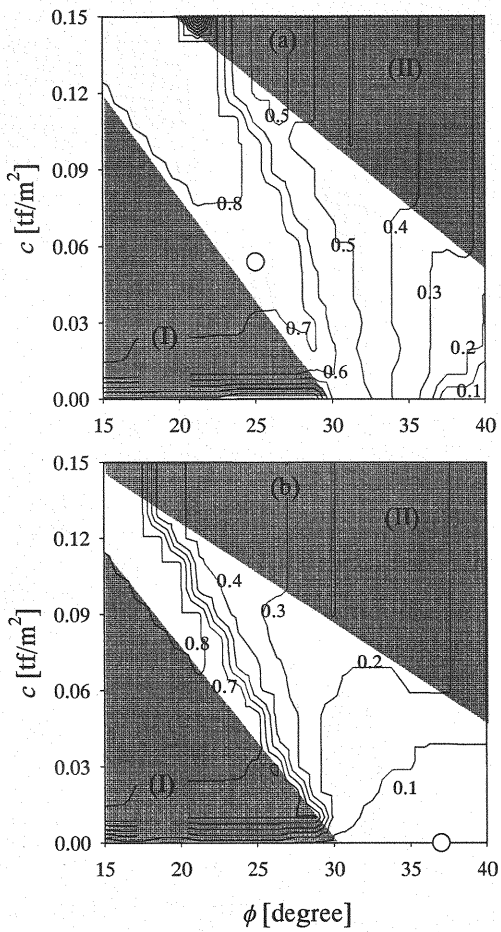

Fig. 7 Calculated relationships between collapse size and soil strength assuming experimental slopes (a: Case 1, b: Case 3, white circles ○ indicate experimental results)

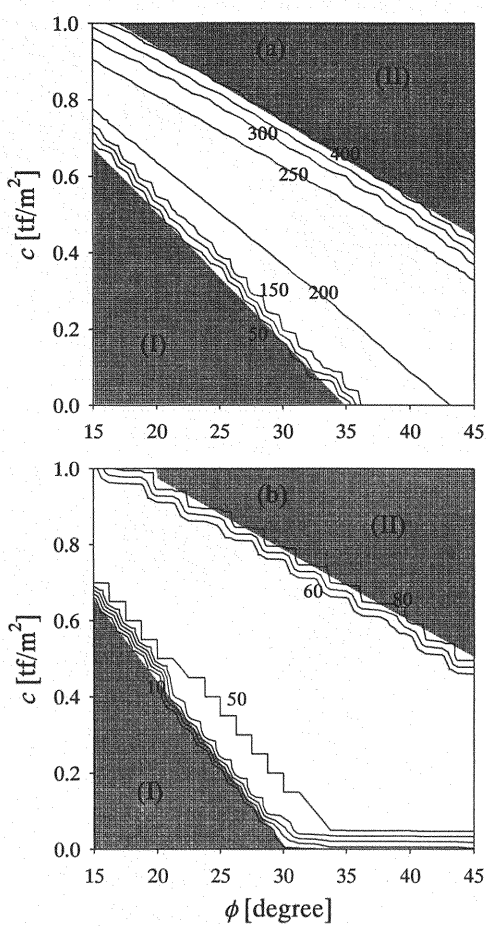

Fig. 8 Calculated relationships between time from rainfall beginning to collapse occurrence and soil strength assuming hypothetical long slope (a: typical forest soil, b: soil sampled at Senokuchi area)

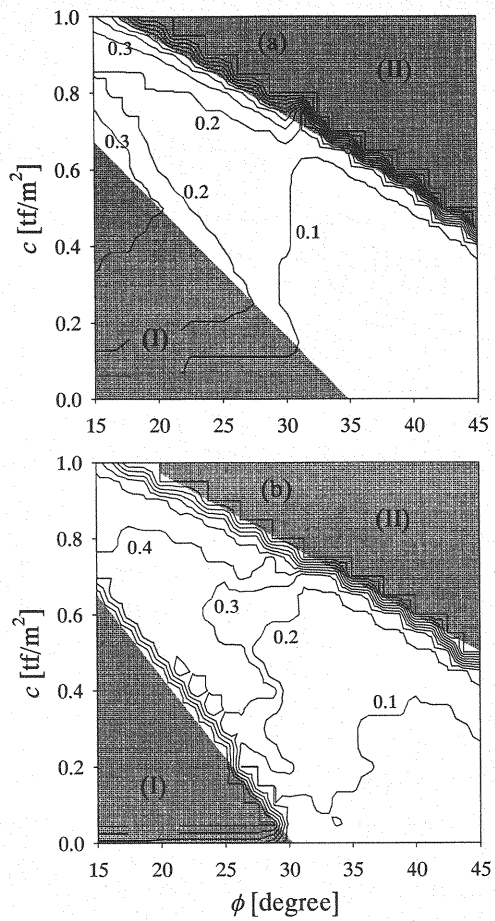

Fig. 9 Calculated relationships between collapse size and soil strength assuming hypothetical long slope (a: typical forest soil, b: soil sampled at Senokuchi area)

CONCLUSION

In the present study, relationship between process of slope failure including the single or multi-phase slope failures and soil properties (soil strength and hydraulic characteristics) was investigated by the physical experiment and the numerical simulation. According to results of the physical experiment and the numerical simulation, it is confirmed that time of landslide occurrence and relative size of first slope failure strongly depend on soil internal friction angle ϕ and cohesion c; relatively small portion at down-slope end of slope with small soil cohesion c and large internal friction angle ϕ tend to collapse, and following multi-phase landslide tend to occur, and relatively large portion of the slope with small soil internal friction angle ϕ and large soil cohesion c tend to collapse at once, and no following failure tends to occur. However, the timing, size and process of landslides also depend on the soil hydraulic properties, bedrock morphology and soil layer thickness, and the mixing effects of these properties are quite complex. Therefore, quantitative relationship between soil internal friction angle ϕ and cohesion c and timing and size of landslides is not clear, yet. It is necessary to elucidate more detailed mechanism of these different landslide processes. It is also necessary to develop a simulation model to demonstrate the multi-phase slope failure by

continuing the soil water infiltration and the slope stability analysis for displaced soil layer after the previous slope failures.

AKNOWLEDGEMENT

We thank Mr. Toshihiko Miyazaki and Mr. Yujiro Hayashi who were students of Graduate School of Engineering, Kyoto University, for their enthusiastic support in the physical experiment and numerical simulation.

REFERENCES

1. Hiura, H., Kaibori, M., Suemine, A., Satofuka, Y. and Tsutsumi, D. : Sediment related disasters in Kisawa Village and Kaminaka Town in Tokushima Prefecture, Japan, induced by the heavy rainfall of the Typhoon Namtheun in 2004 (prompt report), Journal of the Japan Society of Erosion Control Engineering, Vol.57, No.4, pp.39-47, 2004 (in Japanese, with English abstract).
2. Hayashi S., Tsuchiya S., Kondo K., Shibano H., Numamoto S., Kosugi K., Yamakoshi T., Ikeda A.: Sediment related disasters caused by typhoon Meari (T0421) in Miyagawa village, Mie prefecture on September 29, 2004 (prompt report), Journal of the Japan Society of Erosion Control Engineering, Vol.57, No.4, pp.48-55, 2004 (in Japanese, with English abstract).
3. Sabo section in Oita Prefecture Government: Data of natural disasters occurred in 2005, 2005 (in Japanese, the title is tentatively translated by the author).
4. Kosugi, K.: Lognormal distribution model for unsaturated soil hydraulic properties, Water Resources Research, 32, pp.2697-2703, 1996.
5. Kubota, T. and Nakamura, H.: Landslide susceptibility estimation by critical slip surface analysis combined with reliable analysis, Journal of the Japan Landslide Society, Vol.27 (4), pp.18-25, 1991 (in Japanese).

APPENDIX – NOTATION

The following symbols are used in this paper:

a_i = angle of slip surface within i^{th} slice;

c' = cohesion;

c_i' = cohesion of the soil at i^{th} vertical slice;

$C(\psi)$ = soil water capacity;

i = number of vertical slice of soil layer;

K_s = saturated hydraulic conductivity;

$K(\psi)$ = hydraulic conductivity;

l_i = length of slip surface within i^{th} slice;

u_i = water pressure affected on the slip surface at i^{th} slice;

W_i = weight of i^{th} slice;

ϕ' = internal friction angle;

ϕ_i' = internal friction angle of the soil at i^{th} vertical slice;

θ_r = residual volumetric water content;

θ_s = saturated volumetric water content;

σ = a dimensionless parameter related to the width of the pore-size distribution in Lognormal Model;

ψ_m = pressure potential corresponding to the median soil pore radius in Lognormal Model.

(Received Aug 07, 2008 ; revised Jan 23, 2009)